

Effect of chemical short-range order on primary radiation damage in TiVTaNb high-entropy alloys

Yong-Peng Zhao(赵永鹏), Yu-Ze Liu(刘禹泽), Yan-Kun Dou(豆艳坤), Zhong-Ao Zhang(张忠傲), Xin-Fu He(贺新福), and Wen Yang(杨文)

Citation: Chin. Phys. B, 2026, 35 (**2**): 026101. DOI: 10.1088/1674-1056/adf0e5
http://cpb.iphy.ac.cn; http://iopscience.iop.org/cpb

What follows is a list of articles you may be interested in

Sensitivity of short-range order prediction to machine learning potential formalisms: A case study on NbMoTaW high-entropy alloy

Dingyi Jin(金定毅), Guo Wei(魏国), and Haidong Wang(王海东)
Chin. Phys. B, 2025, 34 (**9**): 096104. DOI: 10.1088/1674-1056/ae039a

High-entropy alloys in synergistic electrocatalytic conversion applications

Hui Zhang(张辉), Zhengxiong Liu(刘争雄), Le Fang(方乐), Yin Wang(王音), Shuai Chen(陈帅), and Wei Ren(任伟)
Chin. Phys. B, 2025, 34 (**8**): 086109. DOI: 10.1088/1674-1056/ade8e6

Molecular dynamics study of primary radiation damage in TiVTa concentrated solid-solution alloy

Yong-Peng Zhao(赵永鹏), Yan-Kun Dou(豆艳坤), Xin-Fu He(贺新福), Han Cao(曹晗),Lin-Feng Wang(王林枫), Hui-Qiu Deng(邓辉球), and Wen Yang(杨文)
Chin. Phys. B, 2024, 33 (**3**): 036104. DOI: 10.1088/1674-1056/ad0146

Comparison of formation and evolution of radiation-induced defects in pure Ni and Ni-Co-Fe medium-entropy alloy

Lin Lang(稂林), Huiqiu Deng(邓辉球), Jiayou Tao(陶家友), Tengfei Yang(杨腾飞), Yeping Lin(林也平), and Wangyu Hu(胡望宇)
Chin. Phys. B, 2022, 31 (**12**): 126102. DOI: 10.1088/1674-1056/ac891e

Influence of temperature and alloying elements on the threshold displacement energies in concentrated Ni-Fe-Cr alloys

Shijun Zhao(赵仕俊)
Chin. Phys. B, 2021, 30 (**5**): 056111. DOI: 10.1088/1674-1056/abf10d

---

Effect of chemical short-range order on primary radiation damage in TiVTaNb high-entropy alloys

Yong-Peng Zhao(赵永鹏), Yu-Ze Liu(刘禹泽), Yan-Kun Dou(豆艳坤)†,
Zhong-Ao Zhang(张忠傲), Xin-Fu He(贺新福), and Wen Yang(杨文)

Reactor Engineering Technology Research Division, China Institute of Atomic Energy, Beijing 102413, *China*

(Received 7 May 2025; revised manuscript received 14 July 2025; accepted manuscript online 17 July 2025)

Molecular dynamics simulations were carried out to study the effect of chemical short-range order (CSRO) on the primary radiation damage in TiVTaNb high-entropy alloys (HEAs). We have performed displacement cascade simulations to explore the CSRO effect on the generation and evolution behaviors of irradiation defects. The results demonstrate that CSRO can suppress the formation of Frenkel pairs in TiVTaNb HEAs, with the suppression effect becoming more pronounced as the degree of CSRO increases. CSRO can change the types of interstitial defects generated during cascade collisions. Specifically, as the degree of CSRO increases, the proportion of Ti-related interstitials shows a marked enhancement, primarily evidenced by a significant rise in Ti–Ti dumbbells accompanied by a corresponding decrease in Ti–V dumbbells. CSRO exhibits negligible influence on defect clustering and the nucleation and evolution of dislocation loops. Regardless of CSRO conditions, TiVTaNb HEAs preserve exceptional radiation tolerance throughout the cascade damage process, suggesting that the intrinsic properties of this multi-principal element system dominate its radiation response. These findings provide fundamental insights into the CSRO effect on defect formation and evolution behaviors in HEAs, which may provide new design strategies for high-entropy alloys.

Keywords: high-entropy alloy, chemical short-range order, primary radiation damage, molecular dynamics simulation

PACS: 61.72.J–, 02.70.Ns, 61.82.Bg

DOI: 10.1088/1674-1056/adf0e5 **CSTR:** 32038.14.CPB.adf0e5

1. Introduction

As the demand for more efficient and safer nuclear energy systems grows, the development of robust reactor cladding materials becomes critical. High-entropy alloys (HEAs) have been reported to exhibit exceptional radiation resistance, mechanical strength, and corrosion durability, offering a compelling alternative to conventional reactor cladding materials.[1–3] In particular, body-centered cubic (bcc) HEAs composed of refractory elements exhibit excellent physical properties, attributed to their unique constituent characteristics and core effects, including high entropy, severe lattice distortion, sluggish diffusion, and the cocktail effect.[4–6] Recent studies on TiVTaNb refractory HEAs have demonstrated good thermal stability, mechanical properties, and irradiation resistance.[7–11] In our previous experiment, nanometer-scale triangular Ti-rich precipitates were observed in TiVTaNb HEAs after Ti ion irradiation at 550 °C up to 10 dpa, while the formation mechanisms and influencing factors governing irradiation-induced precipitation still remain unclear.

The atomic-scale formation and evolution of irradiation defects are critical to understanding the mesoscale irradiation damage and macroscale mechanical performance degradation. The primary radiation damage and peculiar point defect properties originating from the multi-principal element effects in TiVTa medium-entropy alloys (MEAs) and TiVTaNb HEAs have been studied in our reported results. It demonstrated that defect formation and migration energies exhibit broad distributions, sluggish defect diffusion was observed in TiVTaNb HEAs.[12–14] Furthermore, the reduction in primary radiation damage was observed due to the enhanced recombination of point defects and the lower binding energies of defect clustering in TiVTa MEAs compared to pure V.[15] However, the influence of chemical short-range order (CSRO), an intrinsic feature in HEAs, on irradiation defect behavior remains unexplored. Despite the high chemical complexity in HEAs, local regions at the microscale may exhibit preferential atomic arrangements due to the differences in atomic size, electronegativity, and chemical bonding, leading to the formation of CSRO. The existence of CSRO has been experimentally confirmed, Chen *et al.*[16] directly observed CSRO in VCoNi MEAs using atomic-resolution transmission electron microscopy and chemical mapping, providing evidence of CSRO through electron diffraction and detailed information on its size, elemental composition, site occupancy, and three-dimensional configuration. CSRO is an intrinsic microstructural feature of HEAs, typically confined to sub-nanometer scales within the first and second nearest-neighbor atomic layers. It plays a crucial role in mechanical properties such as strengthening, strain hardening, and plasticity.[17] Studies suggest that tailoring CSRO may be key to further enhanc-

†Corresponding author. E-mail: douyankun@cnncmail.cn

© 2026 Chinese Physical Society and IOP Publishing Ltd. All rights, including for text and data mining, AI training, and similar technologies, are reserved.

ing the performance of high-entropy alloys, as it can modulate stacking fault energy,[18] promote work hardening,[19] influence corrosion resistance,[20,21] and improve irradiation resistance.[22,23] During irradiation, CSRO affects the formation and migration of point defects, defect clustering, and dislocation motion.[24] The local ordering induced by CSRO directly alters lattice distortions, thereby influencing the behavior of irradiation-induced defects. Additionally, CSRO regions may act as defect trapping centers, impacting the formation of defect clusters.[25]

Chemical short-range order significantly influences the formation and evolution of irradiation defects in HEAs, closely related to defect dynamics during atomic cascade collisions under irradiation. Zhang *et al.*[22] combined ion irradiation experiments and cascade collision simulations to investigate the effect of CSRO on irradiation damage in CrCoNi MEAs. They found that CSRO suppresses defect cluster formation, particularly reducing defect number density. While CSRO minimally affects the formation energy of irradiation-induced point defects, it significantly alters their diffusion behavior, localizing the migration of vacancies and interstitials. CSRO hinders interstitial motion more than vacancy migration, narrowing the diffusion gap between them and enhancing point defect recombination efficiency. Liu *et al.*[24] employed Monte Carlo and molecular dynamics simulations to study CSRO formation and its impact on irradiation defects in CrFeNi MEAs. They confirmed the presence of CSRO, characterized by Cr-rich clusters and Ni–Fe short-range order, where Cr segregation provides nucleation sites for dislocation loops. CSRO increases the migration energy of point defects, suppressing dislocation loop growth. Thus, CSRO promotes dislocation loop nucleation while inhibiting their growth. Xing *et al.*[26] explored the effect of CSRO on elemental diffusion in CrCoNi and MoNbTa MEAs, demonstrating that CSRO suppresses vacancy-mediated diffusion in both systems. Refractory HEAs exhibit greater lattice distortion, leading to significantly different irradiation defect behaviors compared to face-centered cubic structured HEAs.[27,28] Due to the compositional diversity of HEAs, the influence of CSRO on irradiation damage behavior may vary across different materials. Given the limited research on refractory HEAs, it is essential to investigate TiVTaNb HEAs in this context.

In this paper, the effect of chemical short-range order on the primary radiation damage in TiVTaNb HEAs was studied by using the molecular dynamics (MD) method. Displacement cascade simulations were carried out in TiVTaNb HEAs with and without CSRO, and the evolution behaviors of irradiation defects were analyzed. We will organize the remainder of the paper as follows. Section 2 describes the computational methods. In Section 3, the results of the generation and evolution behavior of defects are presented and discussed. Finally, a summary is given in Section 4. These findings can provide fundamental insights into the irradiation defect dynamics in TiVTaNb HEAs.

2. Methodology

Atomistic simulations were performed to study the effect of chemical short-range order on the primary radiation damage in TiVTaNb HEAs by using the large-scale atomic/molecular massively parallel simulator (LAMMPS).[29] The simulations employed a Finnis–Sinclair formalism-based interatomic potential, specifically developed for defects production and evolution studies in Ti–V–Ta–Nb HEAs.[30]

The hybrid Monte Carlo/Molecular Dynamics (MC/MD) method was employed to construct CSRO models in equiatomic TiVTaNb HEAs within an $80a_0 \times 80a_0 \times 80a_0$ simulation box, where the lattice parameter a_0 equals 3.23 Å. The configurations with CSRO can be generated by performing MC swaps between different type atoms, and the Metropolis criterion was used to determine the acceptance of new configuration. The initial random solid solution (RSS) model was performed 100-MC swaps for each pair atoms, followed by up to 100-MD relaxations per iteration at 300 K. The MD timestep was set to 1 fs, and 30 million steps were carried out in total.

The Warren–Cowley parameter (WCP)[31] was calculated to quantify CSRO within the first-nearest neighbor shell:

$$\mathrm{WCP}_{mn} = 1 - \frac{Z_{mn}}{\chi_n Z_m},$$

where Z_{mn} denotes the coordination number of n-type atoms around m-type atoms, Z_m represents the total coordination number of around m-type atoms, and χ_n is the atomic fraction of n-type atoms. Positive WCP_{mn} values indicate depletion of mn-type pairs relative to random distribution, while negative values suggest preferential clustering. A zero value corresponds to a random atomic distribution.

In the cascade collision simulations, we systematically investigated the initial irradiation response of three distinct TiVTaNb configurations: a random solid solution (RSS) model and two CSRO models with varying degrees of chemical ordering. All simulation parameters, except for the initial atomic configurations, were maintained identical across these models. Cascade collision simulations were performed at 300 K with primary knock-on atom (PKA) energies of 5 keV, 10 keV, 20 keV, and 40 keV along the $\langle 135 \rangle$ direction under periodic boundary conditions. For each condition, 30 independent simulations were conducted, and cases involving boundary-crossing atoms were excluded from analysis. Prior to introducing PKA, the system underwent static relaxation followed by dynamic relaxation for 25 ps in the isothermal-isobaric ensemble with a timestep of 0.001 ps. After sufficient relaxation, the PKA was introduced at the box center, and cascade simulations were performed in the microcanonical ensemble using adaptive time steps: 5000 steps at 10^{-4} ps, 10^4 steps at

5×10^{-4} ps, 9500 steps at 0.001 ps, and 8500 steps at 0.01 ps, totaling 100 ps to ensure adequate cascade annealing. Atomic positions and energies were recorded every 500 steps to analyze defect evolution.

The Open Visualization Tool and its included tools[32,33] were used to visualize and analyze the evolution of defects. The formed Frenkel pairs were identified by using the Wigner–Seitz defect analysis, the number of Frenkel pairs N_{FP} as a function of time was monitored for RSS and CSRO models. The defect recombination rate was calculated as $(N_{\mathrm{peak}} - N_{\mathrm{end}})/N_{\mathrm{peak}} \times 100$, where N_{peak} and N_{end} are the peak number and the surviving number of FPs. Then we calculated the agglomeration rates of vacancies and interstitials. Defect clusters were identified using cluster analysis with cut-off radius corresponding to the second- and third-nearest-neighbor distances for vacancy and interstitial clusters, respectively. Structure analysis was performed by using the polyhedral template matching, and the dislocation loops are analyzed by the implemented dislocation extraction algorithm.

3. Results and discussion

3.1. Chemical short-range order in TiVTaNb HEAs

Hybrid MC/MD simulations were carried out to construct configurations with CSRO in TiVTaNb HEAs. As shown in Fig. 1(a), by comparing the configurations between RSS model and high CSRO model, we can clearly observe the aggregation of Ti elements and V–Ta atomic pairs. Figure 1(b) shows the average potential energy evolution along simulation, the energy of supercell exhibits an initial rapid decrease, followed by a gradual decline to reach a steady state, indicating the formation of energetically stable configuration. Figure 1(c) shows the extent of CSRO for different atomic pairs corresponding to different configurations, which are calculated for the first neighbor shell. The initial atomic configuration exhibits a fully random distribution, with all WCP values for atomic pairs being zero. For configurations with CSRO, atomic pairs exhibit formation preferences, albeit to varying degrees. For high CSRO model, we observe negative values of WCP for Ti–Ti (−0.61), V–Ta (−0.35), V–V (−0.34), and Ti–Nb (−0.23), indicating that these pairs are relatively favored. On the contrary, the pairs of Ti–V (0.44), Ti–Ta (0.40), and V–Nb (0.25) are less likely to form, while Ta–Ta pairs (−0.06), Ta–Nb pairs (0.00), and Nb–Nb pairs (−0.02) are randomly distributed within the supercell. In order to evaluate the effect of CSRO degree on irradiation damage behavior, we selected two CSRO configurations for subsequent cascade collision simulations.

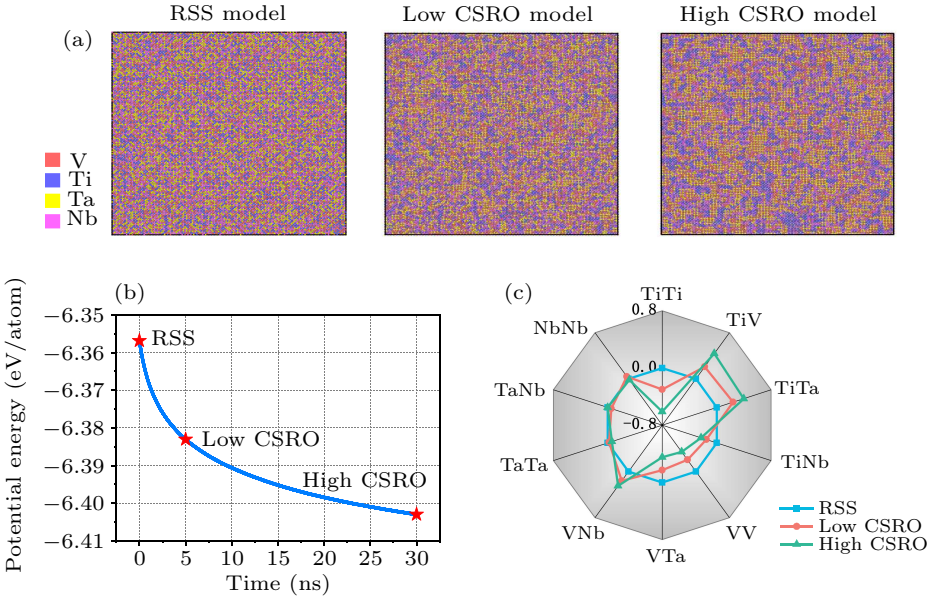


Fig. 1. Atomic configurations, potential energy, and Warren–Cowley parameters of the TiVTaNb HEAs during hybrid MC/MD simulations. Representative configurations of (a) RSS and high CSRO TiVTaNb HEAs. (b) Variation of potential energy with iterations. (c) Warren–Cowley parameters for the RSS, low CSRO, and high CSRO configurations.

3.2. Frenkel pairs

The production and evolution behaviors of defects are of primary interest during cascade simulations. First, by performing Wigner–Seitz analyze, we obtained the evolution of the average number of generated Frenkel pairs during cascade collision simulations with three different PKA energies for RSS, low and high CSRO TiVTaNb HEAs, as shown in Figs. 2(a)–2(c). And the average number of survived Frenkel pairs and defect recombination rate are displayed in Table 1. As exemplified by the 10-keV cascade collision simulations, the introduction of PKA induces rapid generation of Frenkel pairs within the system. The defect population reaches its maximum concentration (thermal spike) at approximately 0.75 ps. Comparative analysis across the three simulated PKA

energies reveals that the random solid solution configuration consistently demonstrates the highest peak defects, followed by the low CSRO configuration, while the high CSRO configuration exhibits the lowest defects at peak. With increasing simulation time, extensive defect recombination led to a significant reduction in Frenkel pairs population, ultimately reaching a stable state at 30 ps with a limited number of surviving defects. Across all three PKA energies investigated, the RSS configuration consistently exhibited the highest stable defect concentration, followed by the low CSRO structure, while the high CSRO configuration maintained the lowest defect retention. Notably, both peak defect concentration and surviving defect population showed identical ranking patterns among the three configurations (RSS > low CSRO > high CSRO), while their defect recombination rates demonstrated no statistically significant differences. Such a trend was found to be unaffected by the PKA energy. Notably, this trend is consistently observed in CrCoNi medium-entropy alloys.[22] Furthermore, our comparative analysis reveals that under identical PKA energies, TiVTaNb HEAs exhibit a significantly higher population of surviving defects than CrCoNi alloys. In a word, CSRO can suppress the formation of Frenkel pairs. The formation and diffusion behavior of point defects govern the generation of Frenkel pairs during cascade collisions. The formation of CSRO alters the local chemical environment of atoms, thereby influencing both the formation and diffusion of point defects. Based on the results shown in Figs. 2(a)–2(c) and Table 1, the difference in the number of surviving Frenkel pairs is primarily attributed to the disparity in peak Frenkel pair counts. We speculate that the distinct nearest-neighbor atomic environments make it more difficult for point defects to form in the CSRO configuration compared to the RSS configuration, ultimately resulting in fewer Frenkel defect pairs in the former.

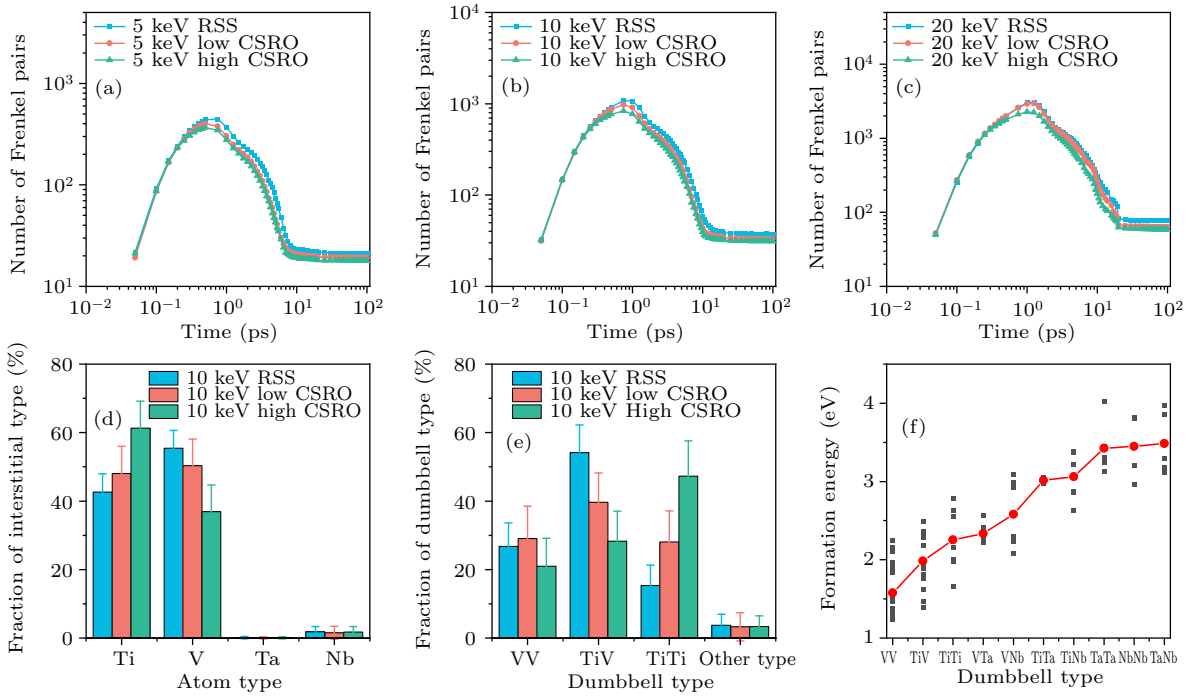


Fig. 2. (a)–(c) Average number of Frenkel pairs *versus* time for cascade collision simulations with different PKA energies (5 keV, 10 keV, 20 keV) for RSS (blue squares), low (red circles), and high CSRO (green triangles) TiVTaNb HEAs. (d)–(e) Fraction of interstitials of a given type in the case of 10-keV cascade simulations. (f) Formation energies of different dumbbells in RSS TiVTaNb HEA calculated by first-principal method in our previous study.[12]

Table 1. Average number of survived Frenkel pairs and defect recombination rate for cascade collision simulations in TiVTaNb HEAs.

PKA energy	Model	Survived Frenkel pairs	Recombination rate (%)
5 keV	RSS	21.2±3.8	95.2±1.0
	low CSRO	19.1±4.1	95.2±0.9
	high CSRO	17.9±3.9	95.0±1.3
10 keV	RSS	37.4±6.6	96.4±0.9
	low CSRO	33.1±6.0	96.6±1.0
	high CSRO	31.2±5.5	95.7±1.4
20 keV	RSS	76.5±16.7	97.3±1.0
	low CSRO	63.2±13.1	97.7±0.7
	high CSRO	58.5±14.5	97.3±0.9

Figures 2(d)–2(f) show the CSRO effect on the type distribution of interstitials formed during cascade simulation in TiVTaNb HEAs. Across all three configurations, the stable interstitial defects generated by cascade collisions are predominantly composed of Ti and V, albeit with varying relative concentrations. These interstitials consistently adopt dumbbell configurations, with V–V, Ti–V, and Ti–Ti dumbbells being the most prevalent, though their proportions differ among the configurations. Notably, increasing chemical short-range order leads to a systematic redistribution of both elemental composition and dumbbell types: (i) the fractional concentration

of Ti interstitials rises while V decreases, with Ta and Nb remaining nearly invariant; (ii) among dumbbell configurations, V–V dumbbells show relatively minimal change, whereas Ti–V fractions decline and Ti–Ti formations increase proportionally. This evolution suggests that CSRO enhances Ti–Ti bonding stability at the expense of mixed Ti–V coordination in the defect structures. In contrast, the populations of other interstitial configurations remain relatively stable, suggesting that CSRO preferentially influences Ti-related defect structures while having minimal impact on other atomic species. This phenomenon can be easily understood by the formation energies of interstitials calculated in our previous study,[12] as shown in Fig. 2(e). In TiVTaNb HEAs, the formation energies of V–V, Ti–V, and Ti–Ti dumbbells are the lowest, followed by V–Ta and V–Nb dumbbells. Ti–Ta and Ti–Nb dumbbells are relatively high, while Ta–Ta, Ta–Nb, and Nb–Nb dumbbells have the highest formation energies. The neighboring atomic environment may determine whether a stable dumbbell can be formed at this position. In the low and high CSRO models, atomic pairs exhibit formation preferences, especially for the preference of Ti–Ti and disfavoring of Ti–V, which is consistent with the distribution of formed interstitials during cascade collisions.

3.3. Defect clusters

The defect clustering behavior in TiVTaNb HEAs with different configurations following cascade collision simulations was presented in Fig. 3 and Table 2.

Table 2. Clustered defect fraction for cascade simulations in TiVTaNb HEAs.

PKA energy	Model	Clustered vacancy fraction	Clustered interstitial fraction
5 keV	RSS	0.36±0.17	0.11±0.07
	low CSRO	0.43±0.13	0.14±0.08
	high CSRO	0.35±0.16	0.15±0.09
10 keV	RSS	0.43±0.14	0.15±0.08
	low CSRO	0.38±0.11	0.16±0.08
	high CSRO	0.43±0.16	0.18±0.01
20 keV	RSS	0.40±0.20	0.07±0.15
	low CSRO	0.47±0.12	0.17±0.07
	high CSRO	0.45±0.10	0.20±0.07

The results demonstrate that both the PKA energy and the degree of CSRO exhibit negligible influence on defect clustering in TiVTaNb HEAs. Variations in PKA energy and initial configurations lead to only minor fluctuations in defect clustering rates, all within the margin of error. Notably, the vacancy agglomeration rate consistently exceeds the interstitial agglomeration rate across all conditions. This observation suggests that CSRO primarily affects the defect formation stage and the distribution of defect types, with minimal impact on clustering behavior. Furthermore, comparative analysis with previous cascade collision simulation results of pure vanadium (V) and TiVTa MEAs using the RSS model reveals significant differences. For instance, at a primary knock-on atom energy of 10 keV, the interstitial agglomeration rate is 0.47±0.13 for pure V, 0.25±0.14 for the TiVTa MEAs, and further reduced to 0.15±0.08 in TiVTaNb HEAs, demonstrating the lowest value

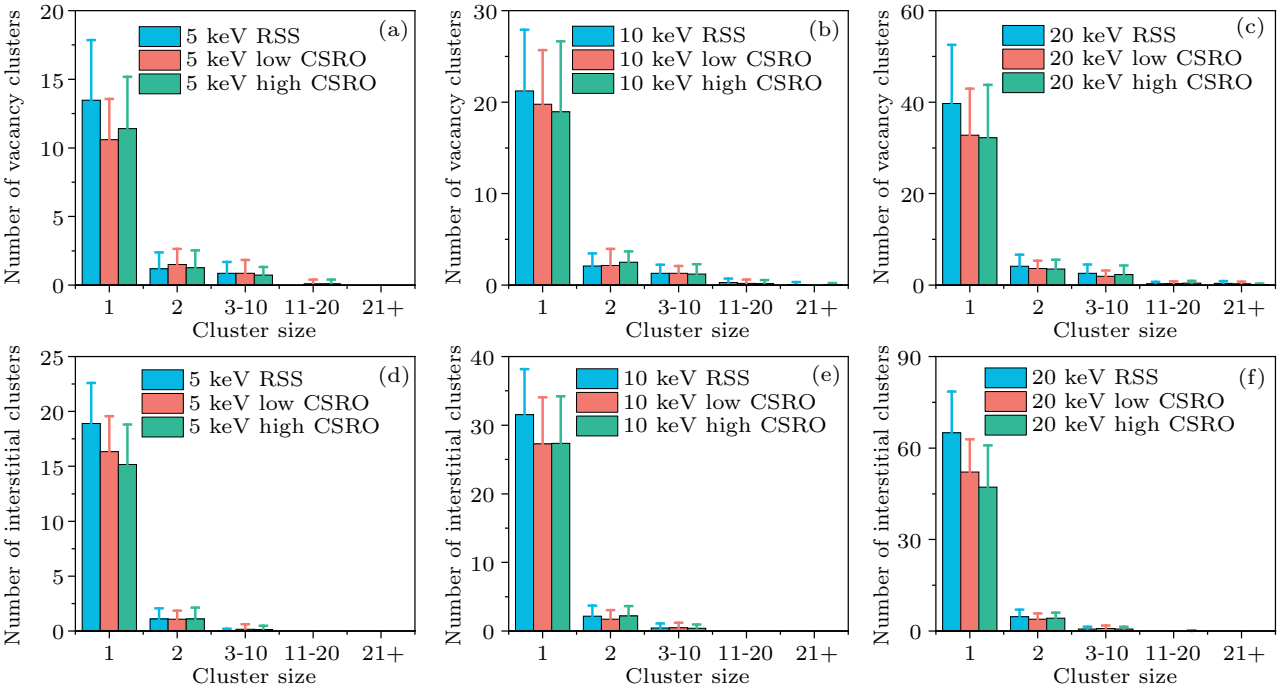


Fig. 3. The number of different size vacancy and interstitial clusters for cascade simulations with different PKA energies (5 keV, 10 keV, 20 keV) for RSS, low and high CSRO TiVTaNb HEAs.

among the studied systems. Similarly, for vacancy clustering, the rates are 0.78±0.10 for pure V, 0.32±0.16 for TiVTa MEAs, and 0.43±0.14 for TiVTaNb HEAs. These results indicate that TiVTaNb HEAs possess both the lowest interstitial agglomeration rate and relatively low vacancy agglomeration rate, highlighting the suppressing effect of multi-principal element characteristics on primary radiation damage. The reduced interstitial agglomeration rate can be attributed to two key factors: retarded interstitial diffusion and lower binding energy. Previous studies have shown that in the temperature range of 500 K–1000 K, TiVTaNb HEA exhibits the lowest interstitial diffusion coefficient compared to V and TiVTa MEAs.[12] Additionally, both interstitial clusters and dislocation loops in TiVTaNb HEA demonstrate the lowest binding energies among these materials.[34]

3.4. Dislocation loops

Following the investigation of the effects of CSRO on Frenkel pairs formation and defect clustering behavior in TiVTaNb HEAs during cascade collisions, we further analyzed the influence of CSRO on dislocation loops formation. In cascade collision simulations with PKA energy up to 20 keV, no dislocation loops were observed in any of the cases. In contrast, pure vanadium already exhibited $1/2\langle 111\rangle$ interstitial and vacancy dislocation loops at 20 keV, primarily due to the formation of fewer point defects and lower defect clustering rates in TiVTaNb HEAs compared to pure vanadium.[15] Our analysis revealed that in cascade simulations with PKA energy up to 40 keV, there were no significant differences in the size, number, or occurrence probability of dislocation loops between random and CSRO configurations of TiVTaNb HEAs, indicating that CSRO has minimal impact on these characteristics of dislocation loops formation. Therefore, this section focuses on the 40 keV simulations of high CSRO TiVTaNb HEA as a representative case. As shown in Fig. 4, we observed the formation of different types of dislocation loops. Figures 4(a)–4(e) and 4(f)–4(j) illustrate the formation processes of $\langle 100\rangle$ and $1/2\langle 111\rangle$ vacancy-type dislocation loops, respectively. Notably, no interstitial-type dislocation loops were detected in any of the simulation cases. Among 30 independent simulations, only three cases exhibited dislocation loop formation, suggesting that dislocation loop nucleation is particularly challenging in TiVTaNb HEAs. This phenomenon was consistently observed in both the RSS model and low CSRO configurations.

At higher PKA energies, the formation of interstitial dislocation loops becomes possible. We speculate that CSRO may influence the relative proportions of different atomic species within interstitial dislocation loops in TiVTaNb HEAs. Future studies could employ additional simulation methods, such as kinetic Monte Carlo or cluster dynamics, to further investigate the influence of CSRO on long-term irradiation damage behavior. Furthermore, recent studies show that local chemical short-range ordering can be tunable, for example via heat treatment, this provides a fascinating avenue for the development of irradiation-resistant HEAs better suited for nuclear applications.

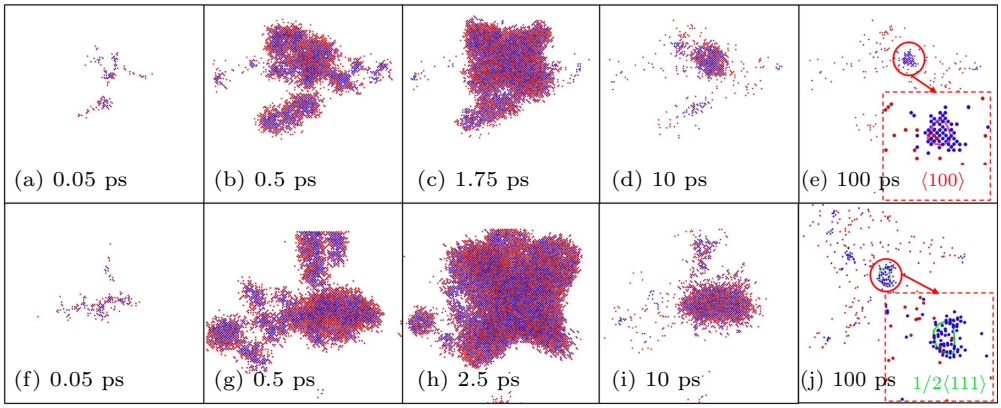


Fig. 4. Representative snapshots of defect distribution for 40-keV cascade collision simulations in high CSRO TiVTaNb HEAs. Panels (a)–(e) and (f)–(j) show the formation processes of $1/2\langle 111\rangle$ and $\langle 100\rangle$ dislocation loop, respectively. Red and blue circles represent interstitials and vacancies.

4. Conclusion

In the present study, the primary radiation damage has been investigated systemically for TiVTaNb HEAs by molecular dynamics simulations. Displacement cascade simulations were carried out to study the production and evolution behaviors of irradiation defects. On the basis of the results presented here and accounting for our previously published data, the following conclusions were obtained.

(i) CSRO can suppress the formation of Frenkel pairs in TiVTaNb HEAs, with the suppression effect becoming more pronounced as the degree of CSRO increases.

(ii) CSRO alters the types of interstitial defects generated during cascade collisions in TiVTaNb HEAs. Specifically, as the degree of CSRO increases, the proportion of Ti-related interstitials shows a marked enhancement, primarily evidenced

by a significant rise in Ti–Ti dumbbells accompanied by a corresponding decrease in Ti–V dumbbells.

(iii) CSRO exhibits negligible influence on defect clustering in TiVTaNb HEAs. Compared to pure V, both vacancies and interstitials exhibit lower agglomeration rates, with interstitial clustering being significantly suppressed relative to pure V and TiVTa MEAs due to the reduced diffusivity and binding energy with interstitial cluster.

(iv) CSRO has minimal effects on the nucleation and evolution of dislocation loops in cascade collisions with PKA energy up to 40 keV. More importantly, TiVTaNb HEAs preserves its exceptional radiation tolerance throughout the cascade damage process regardless of CSRO conditions, suggesting that the intrinsic properties of this multi-principal element system dominate its radiation response.

Acknowledgements

Project supported by the Youth Program of the National Natural Science Foundation of China (Grant No. 12405324), the CNNC Science Fund for Talented Young Scholars (Grant No. 24940), and the CNNC Basic Science Fund (Grant No. 24851).

References

[1] Miracle D B and Senkov O N 2017 *Acta Mater.* **122** 448
[2] Pickering E J, Carruthers A W, Barron P J, Middleburgh S C, Armstrong D E J and Gandy A S 2021 *Entropy* **23** 98
[3] Yu B, Ren Y, Zeng Y, Ma W, Morita K, Zhan S, Lei Y, Lv G, Li S and Wu J 2024 *J. Mater. Sci. Technol.* **29** 2689
[4] Senkov O N, Wilks G B, Miracle D B, Chuang C P and Liaw P K 2010 *Intermetallics* **18** 1758
[5] Senkov O N, Gorsse S and Miracle D B 2019 *Acta Mater.* **175** 394
[6] Dewangan S K, Mangish A, Kumar S, Sharma A, Ahn B and Kumar V 2022 *Eng. Sci. Technol. Int. J.* **35** 101211
[7] Lee C, Song G, Gao M C, Feng R, Chen P and Brechtl J 2018 *Acta Mater.* **160** 158
[8] Jia N, Li Y, Huang H, Chen S, Li D, Dou Y, He X, Yang W, Yin X and Jin K 2021 *J. Nucl. Mater.* **550** 152937
[9] Lee C, Maresca F, Feng R, Chou Y, Ungar T and Widom M 2021 *Nat. Commun.* **12** 5474
[10] Yin X, Dou Y, He X, Jin K, Wang C, Dong Y, Wang H, Zhong W, Xue Y and Yang W 2022 *JOM* **74** 4326
[11] Chen J, Dong Y, Jin K, Wang B and Xue Y 2022 *J. Phys.: Conf. Ser.* **2383** 012136
[12] Zhao Y, Dou Y, He X, Deng H, Wang L and Yang W 2023 *Comput. Mater. Sci.* **218** 111943
[13] Dou Y, Zhao Y, He X, Gao J, Cao J and Yang W 2023 *J. Nucl. Mater.* **573** 154096
[14] Wang L, Zhao Y, Dou Y, He X, Zhang Z, Chen M, Deng H and Yang W 2024 *Crystals* **14** 166
[15] Zhao Y, Dou Y, He X, Cao H, Wang L, Deng H and Yang W 2024 *Chin. Phys. B* **33** 036104
[16] Chen X, Wang Q, Cheng Z, Zhu M, Zhou H, Jiang P, Zhou L, Xue Q, Yuan F, Zhu J, Wu X and Ma E 2021 *Nature* **592** 712
[17] Wu Y, Zhang F, Yuan X, Huang H, Wen X, Wang Y, Zhang M, Wu H, Liu X, Wang H, Jiang S and Lu Z 2021 *J. Mater. Sci. Technol.* **62** 214
[18] Ding J, Yu Q, Asta M and Ritchie R O 2018 *Proc. Natl. Acad. Sci. USA* **115** 8919
[19] Zhang R, Zhao S, Ding J, Chong Y, Jia T, Ophus C, Asta M, Ritchie R O and Minor A M 2020 *Nature* **581** 283
[20] Xie Y, Artymowicz D M, Lopes P P, Aiello A, Wang D, Hart J L, Anber E, Taheri M L, Zhuang H, Newman R C and Sieradzki K 2021 *Nat. Mater.* **20** 789
[21] Scully J R, Inman S B, Gerard A Y, Taylor C D, Windl W, Schreiber D K, Lu P, Saal J E and Frankel G S 2020 *Scr. Mater.* **188** 96
[22] Zhang Z, Su Z, Zhang B, Yu Q, Ding J, Shi T, Lu C, Ritchie R O and Ma E 2023 *Proc. Natl. Acad. Sci. USA* **120** e2218673120
[23] Cao P 2021 *Acc. Mater. Res.* **2** 71
[24] Liu L, Liu X, Du Q, Wang H, Wu Y, Jiang S and Lu Z 2023 *J. Mater. Sci. Technol.* **135** 13
[25] Zhou Y, Shi T, Li J, Wu L, Peng Q and Lu C 2023 *Int. J. Plast.* **171** 103768
[26] Xing B, Wang X, Bowman W J and Cao P 2022 *Scr. Mater.* **210** 114450
[27] Zhao S, Xiong Y, Ma S, Zhang J, Xu B and Kai J 2021 *Acta Mater.* **219** 117233
[28] Shi T, Su Z, Li J, Liu C, Yang J, He X, Yun D, Peng Q, Lu C 2022 *Acta Mater.* **229** 117806
[29] Plimpton S 1995 *J. Comput. Phys.* **117** 1
[30] Qiu R, Chen Y, Liao X, Lin Y, Dou Y, He X, Yang W, Hu W and Deng H 2022 *J Phys.: Condens Matter* **35** 055701
[31] Cowley J M 1950 *Phys. Rev.* **77** 669
[32] Stukowski A 2009 *Model. Simul. Mat. Sci. Eng.* **18** 015012
[33] Stukowski A 2014 *JOM* **66** 399
[34] Qiu R, Chen Y, Liao X, Dou Y, He X, Yang W, Hu W and Deng H 2024 *J. Nucl. Mater.* **599** 155259